

# SCIENTIFIC REPORTS

OPEN

## Carrier density effect on recombination in PTB7-based solar cell

Yutaka Moritomo<sup>1,2</sup>, Kouhei Yonezawa<sup>1</sup> & Takeshi Yasuda<sup>3</sup>

Received: 07 April 2015

Accepted: 03 August 2015

Published: 01 September 2015

Organic solar cells (OSCs) are promising alternatives to the conventional inorganic solar cells due to their low-cost processing and compatibility with flexible substrates. The development of low band-gap polymer, *e.g.*, poly-[[4,8-bis[(2-ethylhexyl)oxy]benzo[1,2-*b*:4,5-*b'*]dithiophene-2,6-diyl] [3-fluoro-2-[(2-ethylhexyl)carbonyl]thieno[3]thiophenediyl]] (PTB7), increases the power conversion efficiency (PCE) in the last decade. Here, we investigated the interrelation between the instantaneous carrier density ( $n$ ) per donor (D)/acceptor (A) interface area and the carrier density ( $n_{\text{collected}}$ ) collected as photocurrent in PTB7/ $C_{70}$  heterojunction (HJ) device. By means of the time-resolved spectroscopy, we confirmed that the exciton-to-carrier conversion process takes place within  $\sim 1$  ps at the D/A interface of the PTB7/ $C_{70}$  HJ device. We further determined the absolute magnitude of  $n$  by combination of the time-resolved and electrochemical spectroscopies. We found that the carrier recombination becomes dominant if  $n$  exceeds a critical concentration ( $n_c = 0.003$  carriers/nm<sup>-2</sup>). We confirmed that a similar behaviors is observed in the PTB7/[6,6]-phenyl  $C_{71}$ -butyric acid methyl ester (PC<sub>71</sub>BM) bulk heterojunction (BHJ) device. Our quantitative investigation based on the HJ device demonstrates that the fast carrier escape from the D/A interface region is indispensable for high PCE, because the carrier accumulation nonlinearly accelerates the carrier recombination process.

In OSCs, the carriers are produced by the exciton dissociation at the D/A interface in the active layer, reflecting the weak screening effect and/or strong exciton effect (Frenkel exciton)<sup>1</sup>. In other words, the carriers are localized at the interface at the initial stage of the photovoltaic process. This makes a sharp contrast with the conventional inorganic solar cells (ISCs): The carriers are produced at every positions of the active layer, reflecting the strong screening effect and/or weak exciton effect (Wannier exciton). Then, the quantitative determination of the branching ratio between the carrier recombination at the interface region and the carrier escape from the region is indispensable for true comprehension of the photovoltaic process of OSCs. The escaped carriers will be collected at the collector electrodes. We propose that we can quantitatively investigate the carrier recombination/escape branching ratio by preparing the instantaneous dense carrier states by photo-excitation with femtosecond light pulses. Especially, in the HJ device, the instantaneous carrier density ( $n$ ) per D/A interface area can be determined because the interface area is the same as the device area.

BHJ-type OSCs<sup>2,3</sup>, in which nano-level mixture of electron-donating polymer and electron-accepting fullerene-derivative provides a wide exciton-dissociative region within the active layer, show high PCEs and are promising alternatives to the conventional ISCs. Especially, the development of low band-gap polymer, *e.g.*, PTB7, increases the PCE up to 9%<sup>4-6</sup> in the last decade<sup>7,8</sup>. The increase in PCE stimulates extensive time-resolved spectroscopic investigations of the low-band gap OSCs to reveal the carrier formation process<sup>9-12</sup>. The femtosecond time-resolved spectroscopy is a powerful tool to reveal the carrier

<sup>1</sup>Graduate School of Pure and Applied Science, Univ. of Tsukuba, Tsukuba 305-8571, Japan. <sup>2</sup>Center for Integrated Research in Fundamental Science and Engineering (CiRFSE), Univ. of Tsukuba, Tsukuba 305-8571, Japan.

<sup>3</sup>Photovoltaic Materials Unit, National Institute for Materials Science (NIMS), Tsukuba, Ibaraki 305-0047, Japan. Correspondence and requests for materials should be addressed to Y.M. (email: moritomo.yutaka.gf@u.tsukuba.ac.jp)

formation process, because the spectroscopy monitors the relative numbers of the photo-created excitons and carriers in the time domain. Significantly, the spectroscopy decouples the carrier formation and transfer processes, because the former process completes within several ps. Actually, the exciton-to-carrier conversion process in PTB7/PC<sub>71</sub>BM blend film completes in 0.2–0.5 ps<sup>9,10</sup>. Recently, a spectroscopic method<sup>13</sup> was proposed to evaluate the carrier formation efficiency ( $\Phi_{CF}$ ).  $\Phi_{CF}$  is defined by  $n_{\text{formed}}/n_{\text{photon}}$ , where  $n_{\text{formed}}$  ( $n_{\text{photon}}$ ) is the density of the instantaneously formed carriers (absorbed photons) per unit area of the device.  $n_{\text{formed}}$  includes the weakly-bound state of the carriers. Absolute magnitude of  $n_{\text{formed}}$  can be estimated by the combination of the time-resolved and electrochemical spectroscopies.  $\Phi_{CF}$  is the same as the exciton quenching efficiency, if all the quenched excitons are converted to carriers.

In this paper, we investigated the branching ratio between the carrier recombination at the interface region and the carrier escape from the region in the PTB7/C<sub>70</sub> HJ device. By means of the time-resolved spectroscopy, we confirmed that the exciton-to-carrier conversion process takes place within ~1 ps at the D/A interface in the PTB7/C<sub>70</sub> HJ device. In the PTB7/C<sub>70</sub> HJ device,  $\Phi_{CF}$  (=0.56) is nearly constant against the excitation pulse energy ( $I_{\text{photon}}$ ) per unit area of the device while the internal quantum efficiency ( $\Phi_{IQ}$ ) steeply decreases with increase in  $I_{\text{photon}}$  beyond 0.8  $\mu\text{J}/\text{cm}^2$ . We further determined the interrelation between the instantaneous carrier density ( $n$ ) per D/A interface area and the carrier density ( $n_{\text{collected}}$ ) collected as photocurrent. We found that the carrier recombination becomes dominant if  $n$  exceeds a critical concentration ( $n_c = 0.003$  carriers/nm<sup>2</sup>). A phenomenological rate equation with the carrier recombination term ( $-\alpha n^3$ ) well reproduces the experimental relation between  $n$  and  $n_{\text{collected}}$ . We confirmed that a similar behavior is observed in the PTB7/PC<sub>71</sub>BM BHJ device even though  $n_c$  is considered to be much lower than the value of the HJ device.

## Results

**Pulse energy dependence of  $\Phi_{IQ}$  of PTB7-based OSCs.** We fabricated the two types of the PTB7-based OSCs: PTB7/C<sub>70</sub> HJ solar cell with a structure of indium tin oxide (ITO)/poly-(3,4-ethylenedioxythiophene) (PEDOT): poly-(styrenesulfonate) (PSS) (40 nm)/PTB7 (18 nm)/C<sub>70</sub> (25 nm)/bathocuproine (BCP) (5 nm)/MgAg and PTB7/PC<sub>71</sub>BM BHJ cell with a structure of ITO/PEDOT:PSS (40 nm)/active layer (89 nm)/LiF (1 nm)/Al. We measured current ( $I$ )—voltage ( $V$ ) curves (see Supplementary Fig. S1 online) of the two OSCs. The HJ device exhibits an open circuit voltage ( $V_{oc}$ ) of 0.68 V, a short circuit current ( $J_{sc}$ ) of 5.9 mA/cm<sup>2</sup>, a fill factor (FF) of 0.68, and a PCE of 2.7%, while BHJ device exhibits a  $V_{oc}$  of 0.74 V, a  $J_{sc}$  of 17.7 mA/cm<sup>2</sup>, a FF of 0.65, and a PCE of 8.5%. The FF value (=0.68) of the HJ device is slightly higher than that (=0.65) of the BHJ device. The suppressed FF value of the BHJ device is ascribed to the efficient carrier recombination during the carrier transfer process, reflecting the nano-level mixing of the D and A domains. We measured incident photon-to-current conversion efficiency (IPCE) spectra (see Supplementary Fig. S2 online) of the two OSCs. The IPCE of the HJ device is nearly the half of that of the BHJ device. The suppression is ascribed to the thinner active layer (43 nm) of the HJ device as compared with that (89 nm) of the BHJ device. The thinner active layer is further responsible for the lower PCE and  $J_{sc}$  values of the HJ device.

Figure 1a shows  $I$  against  $I_{\text{photon}}$  of femtosecond light pulse at 400 nm in the PTB7-based HJ and BHJ devices. In both the devices, the magnitude of  $I$  linearly increases with  $I_{\text{photon}}$  in the low- $I_{\text{photon}}$  region below ~0.2  $\mu\text{J}/\text{cm}^2$ . However,  $I$  becomes nearly constant (~0.03 mA/cm<sup>2</sup>) above ~2  $\mu\text{J}/\text{cm}^2$ . A similar saturation of  $I$  against  $I_{\text{photon}}$  is observed in P3HT/PCBM BHJ device<sup>14</sup>. Figure 1b shows  $\Phi_{IQ}$  at 400 nm against  $I_{\text{photon}}$ . The magnitudes of  $\Phi_{IQ}$  were evaluated from  $I$  and  $I_{\text{photon}}$  with considering the absorption indexes: 0.61 and 0.84 for HJ and BHJ devices, respectively. In the HJ device (open circles), the  $\Phi_{IQ}$  value (~0.4) in the low- $I_{\text{photon}}$  region is nearly the same as the value (=0.59) determined under 400 nm monochromatic radiation of 6.6 mW/cm<sup>2</sup>. The  $\Phi_{IQ}$  value exponentially decreases with increase in  $I_{\text{photon}}$  beyond 0.8  $\mu\text{J}/\text{cm}^2$ . In the BHJ device (closed circles), the  $\Phi_{IQ}$  value (~0.6) in the low- $I_{\text{photon}}$  region is close to the value (=0.79) determined under 400 nm monochromatic radiation of 6.6 mW/cm<sup>2</sup>. The  $\Phi_{IQ}$  value exponentially decreases with increase in  $I_{\text{photon}}$  beyond 0.2  $\mu\text{J}/\text{cm}^2$ .

**Carrier formation dynamics in PTB7/C<sub>70</sub> heterojunction.** We investigated  $\Delta\text{OD}$  spectra of PTB7/C<sub>70</sub> bilayer, PC<sub>71</sub>BM neat, and PTB7 neat films at 400 nm (see Supplementary Fig. S3 online). The  $\Delta\text{OD}$  spectra of the PC<sub>71</sub>BM (PTB7) neat film show a characteristic photoinduced absorption (PIA), which should be ascribed to the acceptor exciton ( $A^*$ ) [donor exciton ( $D^*$ )]. The  $\Delta\text{OD}$  spectra of the PTB7/C<sub>70</sub> bilayer film show a broad PIA centered at 1150 nm. In the late stage (>10 ps), the profile of the PIA is essentially unchanged. In addition, the spectral profile is similar to that of the doping-induced spectrum of the PTB7 neat film (see Supplementary Fig. S4 online). Therefore, we ascribed the PIA to the photo-created donor carriers ( $D^+$ ). In the early state (<10 ps), however, an additional absorption component is observed around 1500 nm. The additional component should be ascribed to the PIAs due to  $A^*$  and  $D^*$ . We decomposed the  $\Delta\text{OD}$  spectra ( $\phi_{\text{exp}}$ ) of the PTB7/C<sub>70</sub> bilayer film into the components of  $A^*$  ( $\phi_{A^*}$ ),  $D^*$  ( $\phi_{D^*}$ ), and  $D^+$  ( $\phi_{D^+}$ ). The  $\Delta\text{OD}$  spectra of the PC<sub>71</sub>BM (PTB7) neat film at 1 ps was regarded as  $\phi_{A^*}$  ( $\phi_{D^*}$ ) while the  $\Delta\text{OD}$  spectra of the PTB7/C<sub>70</sub> bilayer film at 10 ps was regarded as  $\phi_{D^+}$ . The spectral weights of the respective components were evaluated by least-squares fitting of the observed spectra ( $\phi_{\text{exp}}$ ) with the linear combination of  $\phi_{A^*}$ ,  $\phi_{D^*}$ , and  $\phi_{D^+}$ :  $\phi_{\text{cal}} = C_{A^*}\phi_{A^*} + C_{D^*}\phi_{D^*} + C_{D^+}\phi_{D^+}$ .

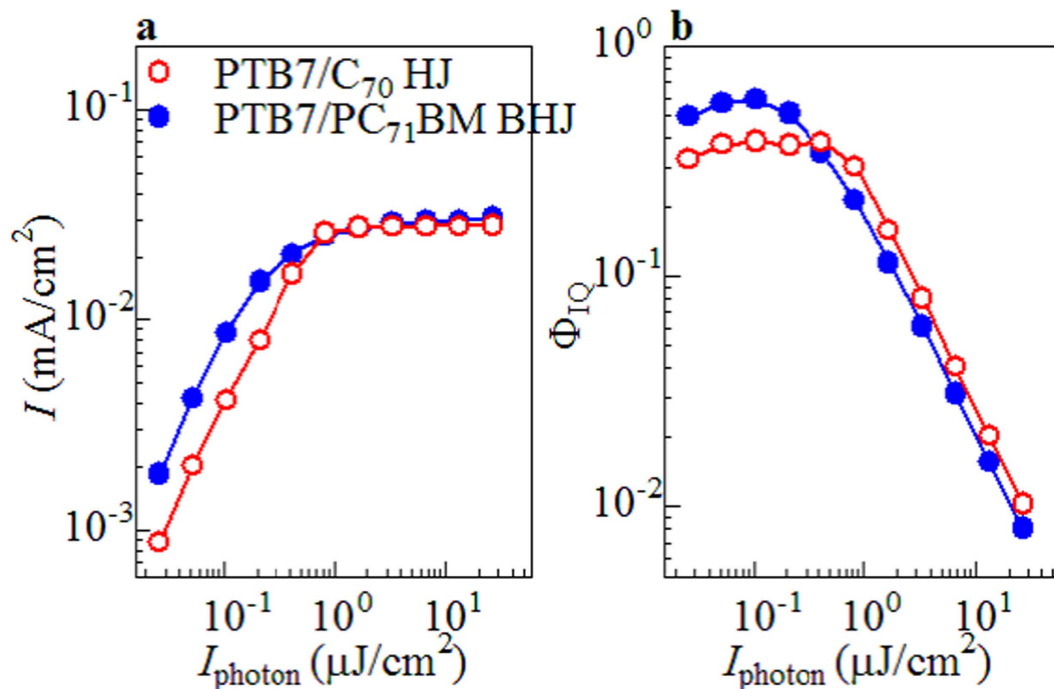


**Figure 1.** (a) Photocurrent ( $I$ ) against energy ( $I_{\text{photon}}$ ) of femtosecond light pulse at 400 nm in the PTB7/ $C_{70}$  HJ and PTB7/ $PC_{71}$ BM BHJ devices. (b)  $\Phi_{IQ}$  against  $I_{\text{photon}}$ . The magnitudes of  $\Phi_{IQ}$  were estimated with considering the absorption indexes: 0.61 and 0.84 for HJ and BHJ devices, respectively. The curves are merely the guides to the eyes.

The coefficients,  $C_{A^*}$ ,  $C_{D^*}$  and  $C_{D^+}$ , were determined so that the evaluation function,  $F(C_{A^*}, C_{D^*}, C_{D^+}) = \sum_i (\phi_{\text{exp}} - \phi_{\text{cal}})^2$ , becomes the minimum. Figure 2a show an example of the spectral decomposition at 0.9 ps. We clearly observed that the photo-excitation at 400 nm excites  $D^*$  in addition to  $A^*$ .

Now, let us evaluate the absolute numbers of the acceptor exciton ( $n_{A^*}$ ), donor exciton ( $n_{D^*}$ ) and donor carrier ( $n_{D^+}$ ) per absorbed photon from the  $\Delta OD$  spectra of the PTB7/ $C_{70}$  bilayer film. For this purpose, we need the spectral intensities,  $\alpha_{A^*}$ ,  $\alpha_{D^*}$ , and  $\alpha_{D^+}$ , per unit densities of  $A^*$ ,  $D^*$ , and  $D^+$ . In order to determine  $\alpha_{A^*}$  and  $\alpha_{D^*}$ , we assumed that one absorbed photon creates one  $A^*$  ( $D^*$ ) in the  $PC_{71}$ BM (PTB7) neat film. We determined  $\alpha_{A^*}$  ( $\alpha_{D^*}$ ) with use of the  $\Delta OD$  spectra of  $PC_{71}$ BM (PTB7) neat film (see Supplementary Fig. S3 online):  $\alpha_{A^*}$  ( $\alpha_{D^*}$ ) is evaluated to be  $0.002 \text{ nm}^2/\text{photons}$  ( $0.020 \text{ nm}^2/\text{photons}$ ) with considering absorption indexes. Then,  $n_{A^*}$  ( $n_{D^*}$ ) is calculated by  $(I_{A^*}/n_{\text{photon}})/\alpha_{A^*}$  [ $(I_{D^*}/n_{\text{photon}})/\alpha_{D^*}$ ], where  $I_{A^*}$  ( $I_{D^*}$ ) and  $n_{\text{photon}}$  are the intensity of the ( $A^*$ ) ( $D^*$ ) component in the PTB7/ $C_{70}$  bilayer film and the absorbed photon number per unit density of the device. The magnitude of  $\alpha_{D^+}$  was determined from the electrochemical differential ( $\Delta OD_{EC}$ ) spectrum (see Supplementary Fig. S4 online).  $\alpha_{D^+}$  is evaluated to be  $0.013 \text{ nm}^2/\text{carriers}$  with use of the doped carrier density. Then,  $n_{D^+}$  is calculated by  $(I_{D^+}/n_{\text{photon}})/\alpha_{D^+}$ , where  $I_{D^+}$  is the intensity of the  $D^+$  component in the PTB7/ $C_{70}$  bilayer film. The magnitudes of  $I_{A^*}$ ,  $I_{D^*}$ , and  $I_{D^+}$  were evaluated by the spectral decomposition of the  $\Delta OD$  spectra into the  $A^*$ ,  $D^*$ , and  $D^+$  components, as exemplified in Fig. 2a.

Figure 2b shows the absolute numbers of  $A^*$  ( $n_{A^*}$ ),  $D^*$  ( $n_{D^*}$ ) and  $D^+$  ( $n_{D^+}$ ) per an absorbed photon against the delay time. The  $n_{A^*}$  values significantly scatter reflecting the small cross section of  $A^*$  ( $\alpha_{A^*} = 0.002 \text{ nm}^2/\text{photons}$ ). Nevertheless, we observed steep decreases in  $n_{A^*}$  and  $n_{D^*}$  with time. The decay times ( $\tau_{\text{decay}}$ ) of  $n_{A^*}$  and  $n_{D^*}$  are roughly evaluated to be 3.1 and 1.6 ps, respectively. On the other hand,  $n_{D^+}$  exponentially increases with the rise time ( $\tau_{\text{rise}}$ ) of 1.0 ps. The rather slow decay time ( $\tau_{\text{decay}} = 3.1 \text{ ps}$ ) of  $A^*$  suggests that the late decay component ( $>1 \text{ ps}$ ) of  $A^*$  does not contribute to the carrier formation. Actually, the sum of the initial exciton number, *i.e.*,  $n_{A^*} + n_{D^*}$  ( $\sim 0.7/\text{photon}$ ) is slightly larger than the carrier number ( $n_{D^+} \sim 0.5/\text{photon}$ ). Thus, the exciton-to-carrier conversion process in the PTB7/ $C_{70}$  bilayer film takes place at the D/A interface within  $\sim 1 \text{ ps}$ . The carrier formation time ( $\sim 1 \text{ ps}$ ) in the PTB7/ $C_{70}$  bilayer film is longer than that ( $= 0.2\text{--}0.5 \text{ ps}$ ) of PTB7/ $PC_{71}$ BM blend film<sup>10</sup>. The longer conversion time is ascribed to be the longer exciton diffusion to the D/A interface in the HJ device than that in the BHJ device.

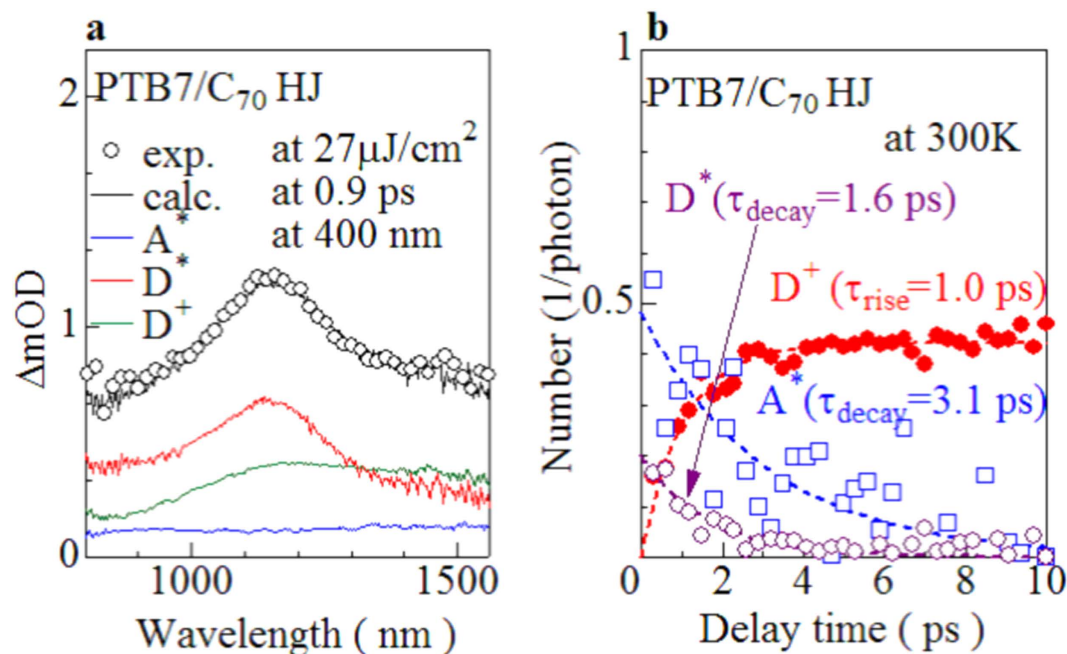


**Figure 2.** (a)  $\Delta OD$  spectra (open circles) of PTB7/C<sub>70</sub> bilayer film at 0.9 ps and at 400 nm together with the spectral decomposition into acceptor exciton (A\*: blue curve), donor exciton (D\*: green curve), and donor carrier (D<sup>+</sup>: red curve) components. The  $\Delta OD$  spectra of the PC<sub>71</sub>BM neat, PTB7 neat, and PTB7/C<sub>70</sub> bilayer films at 1, 1, and 10 ps are regarded as the A\*, D\*, and D<sup>+</sup> components, respectively. (b) Absolute number of acceptor exciton ( $n_{A^*}$ ), donor exciton ( $n_{D^*}$ ) and donor carrier ( $n_{D^+}$ ) per an absorbed photon against the delay time. The magnitudes of  $n_{A^*}$ ,  $n_{D^*}$  and  $n_{D^+}$  were evaluated by the spectral decomposition of the  $\Delta OD$  spectra of the PTB7/C<sub>70</sub> bilayer film. The solid curves are results of the least-squares fittings with an exponential function.

**Pulse energy dependence of  $\Phi_{CF}$  in PTB7-based OSCs.** Next, we investigated pulse energy dependence of the  $\Delta OD$  spectra at 10 ps of the PTB7/C<sub>70</sub> bilayer and PTB7/PC<sub>71</sub>BM blend films at 400 nm (see Supplementary Fig. S5 online). The magnitude of  $\Phi_{CF}$  ( $=\alpha_{\text{photon}}/\alpha_{D^+}$ ) can be calculated from the two quantities.  $\alpha_{\text{photon}}$  ( $=I_{D^+}/n_{\text{photon}}$ ) is the spectral intensities due to D<sup>+</sup> per unit density of absorbed photons.  $\alpha_{D^+}$  is reported to be 0.013 nm<sup>2</sup>/carriers for PTB7<sup>13</sup>. In the PTB7-based OSCs, the carrier formation time is less than 1 ps. Therefore, we evaluated the  $\alpha_{D^+}$  values from the  $\Delta OD$  spectra at 10 ps of the PTB7/C<sub>70</sub> bilayer and PTB7/PC<sub>71</sub>BM blend films with considering the absorption indexes: 0.37 and 0.60 for the bilayer and blend films, respectively. Thus obtained  $\Phi_{CF}$  values are plotted in Fig. 3 together with  $\Phi_{IQ}$  against  $I_{\text{photon}}$ . We found that  $\Phi_{CF}$  ( $=0.56$ ) is nearly independent of  $I_{\text{photon}}$  in the PTB7/C<sub>70</sub> bilayer film even though  $\Phi_{CF}$  at  $I_{\text{photon}} < 2 \mu\text{J}/\text{cm}^2$  is difficult to determine. This makes a sharp contrast with a steep decrease in  $\Phi_{IQ}$  with increase in  $I_{\text{photon}}$  beyond  $0.8 \mu\text{W}/\text{cm}^2$ . A similar behavior of  $\Phi_{IQ}$  and  $\Phi_{CF}$  is observed in the PTB7/PC<sub>71</sub>BM BHJ device. In the high- $I_{\text{photon}}$  region, most of the carriers recombine and do not contribute to the photocurrent ( $\Phi_{IQ} \ll 1$ ). We note that the carrier recombination process takes several nanoseconds in both the devices (see Supplementary Fig. S6 online). We tentatively evaluate the decay times ( $\tau_{\text{decay}}$ ) by least-squares fittings with exponential functions, *i.e.*,  $\Delta mOD = A \exp(-t/\tau)$ :  $\tau_{\text{decay}} = 3.4$  and 5.8 ns for the HJ and BHJ devices, respectively.

Here, we define the instantaneous carrier density ( $n$ ) per unit area of the D/A interface. In the HJ device, the magnitude of  $n$  is the same as  $n_{D^+}$  ( $=n_{\text{photon}} \times \Phi_{CF}$ ) because the D/A interface area is the same as the device area. In the BHJ device, however, the magnitude of  $n$  is smaller than  $n_{D^+}$  because the interface area is much wider than the device area. Under the femtosecond pulse excitation, the carriers are instantaneously produced at the D/A interface before they start migration toward the collector electrodes. Actually, the carriers are generated at the D/A interface within  $\sim 1$  ps. For example, the local carrier density ( $n$ ) at the interface of the HJ device is  $\sim 0.1$  carriers/nm<sup>2</sup> at  $10 \mu\text{J}/\text{cm}^2$ . Under a conventional continuous wave (CW) excitation, however, the carrier migration effectively reduces the  $n$  value. For example, the local carrier density at the interface is  $\sim 10^{-2}$  carriers/nm<sup>2</sup> at  $100 \text{ mW}/\text{cm}^2$  if the carrier escape time from the interface region is 1 ns. On the other hand, it becomes  $\sim 1$  carriers/nm<sup>2</sup> at  $100 \text{ mW}/\text{cm}^2$  with the carrier lifetime of  $\sim 1$  ms, which is comparable to the value ( $\sim 0.1$  carriers/nm<sup>2</sup>) under the femtosecond pulse excitation at  $10 \mu\text{J}/\text{cm}^2$ . These arguments indicate that the significant carrier recombination efficiency observed in the high- $I_{\text{photon}}$  region should be ascribed to the local dense carriers at the interface. In other words, the carriers at the interface region are amenable to the recombination while the carriers escaped from the region are free from the recombination.

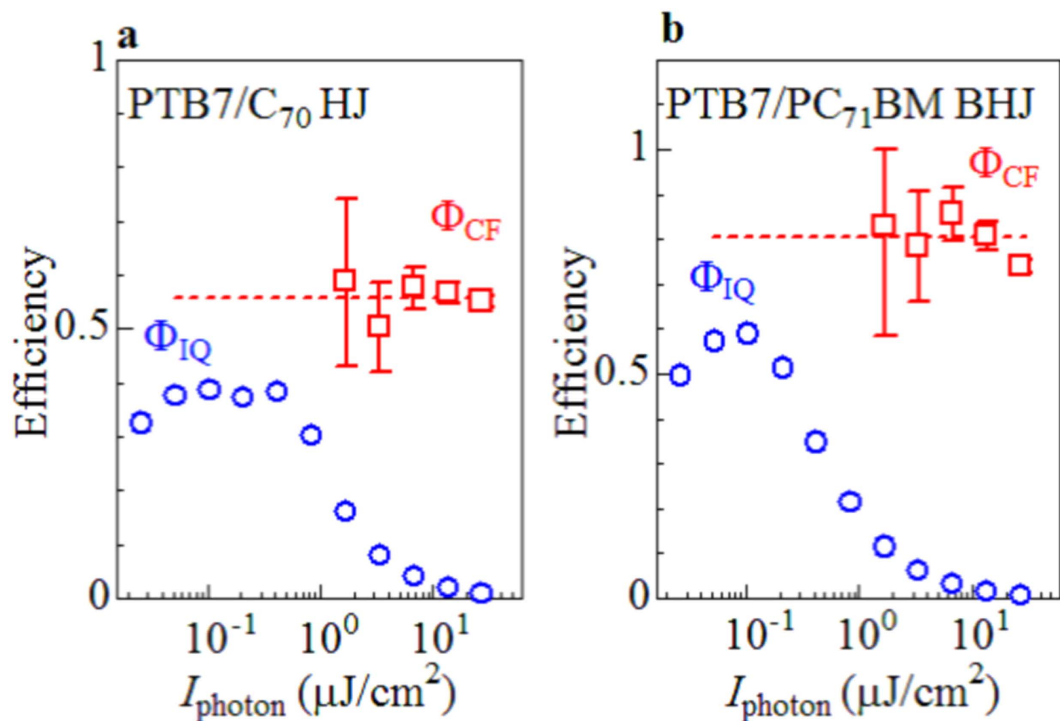


**Figure 3.**  $\Phi_{\text{CF}}$  and  $\Phi_{\text{IQ}}$  of (a) PTB7/C<sub>70</sub> HJ and (b) PTB7/PC<sub>71</sub>BM BHJ devices against energy ( $I_{\text{photon}}$ ) of femtosecond light pulse at 400 nm. The magnitudes of  $\Phi_{\text{CF}}$  were estimated with considering the absorption indexes: 0.37 and 0.60 for the bilayer and blend films, respectively. The error bars of  $\Phi_{\text{CF}}$  were roughly evaluated from the signal/noise ratio of the femtosecond time-resolved spectra. The magnitudes of  $\Phi_{\text{IQ}}$  were estimated with considering the absorption indexes: 0.61 and 0.84 for HJ and BHJ devices, respectively. The broken lines are merely the guide to the eyes.

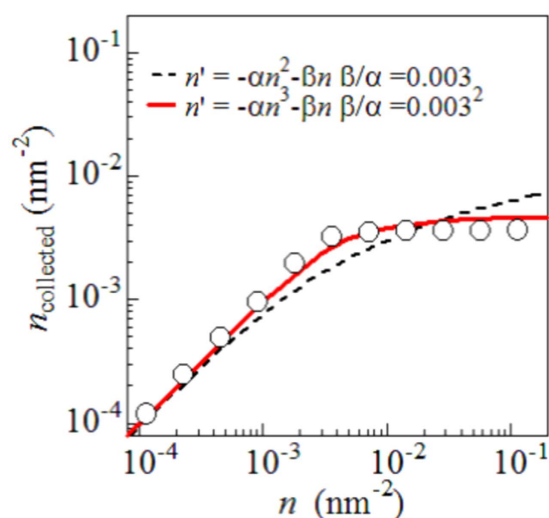


**Figure 4.** Carrier density ( $n_{\text{collected}}$ ) collected as photocurrent against instantaneous carrier density ( $n$ ) per unit area of the D/A interface in PTB7/C<sub>70</sub> HJ device. The  $n$  values were evaluated with assuming constant  $\Phi_{\text{CF}}$  ( $=0.56$ ). The solid and broken curves are drawn by a phenomenological model (see text).

## Discussion

Figure 4 shows the carrier density ( $n_{\text{collected}}$ ) collected as photocurrent against  $n$  ( $=\Phi_{\text{CF}} \times n_{\text{photon}}$ ) in the HJ device. The  $n$  values were evaluated with assuming constant  $\Phi_{\text{CF}}$  ( $=0.56$ ). In the dilute- $n$  region, the photocurrent is proportional to  $n$ . In the dense- $n$  region, however, the photocurrent becomes nearly constant. This suggests that there exists a critical carrier density ( $n_c = 0.003$  carriers/ $\text{nm}^2$ ) above which

the carrier recombination becomes dominant. The  $n_c$  value ( $=0.003$  carriers/nm<sup>2</sup>) corresponds to the value, in which one carrier exists every  $18 \times 18$  nm<sup>2</sup> squares. To quantitatively analyze the carrier recombination kinetics against  $n$ , we adopted a phenomenological rate equation:  $dn/dt = -\alpha n^N - \beta n$ . The first and second terms represent the carrier recombination and the carrier escape from the interface region. The first term at  $N=2$  describes the conventional electron–hole recombination process. The ratio between the coefficients,  $\alpha$  and  $\beta$ , should be fixed as  $\beta/\alpha = n_c^{N-1}$ , because the first and the second terms become comparable at  $n = n_c$ . We assume that all the escaped carriers contribute the photocurrent, *i.e.*,  $n_{\text{collected}} = \int \beta n dt$ . The solid and broken curves in Fig. 4 are results of the phenomenological model at  $N=3$  and 2, respectively. We found that the curve at  $N=3$  excellently reproduces the experiment data. The deviation from the conventional  $n^2$ -dependence ( $N=2$ ) is probably ascribed to the electric double layer effect at the interface, which may cause a many-body interaction between the carriers. Here, we note that the recombination/escape branching ratio is determined by the ratio not by the magnitudes of the coefficients,  $\alpha$  and  $\beta$ . The magnitude determines only the time scale of the branching kinetics. That is, we have no adjustable parameter in this phenomenological mode.

A similar relation between  $n$  and  $n_{\text{collected}}$  is observed in the PTB7/PC<sub>71</sub>BM BHJ device even though we cannot evaluate the magnitude of  $n$ . Alternatively, we estimated the critical carrier density ( $n_c' = 0.002$  carriers/nm<sup>2</sup>) per unit area of the device, above which the carrier recombination becomes dominant. We note that  $n_c$  (per unit area of the interface) is much smaller than  $n_c'$  (per unit area of the device) because the D/A interface area is much wider than that of the device area. That is,  $n_c$  of the BHJ device is much lower than  $n_c$  ( $=0.003$  carriers/nm<sup>2</sup>) of the HJ device. We ascribe the suppressed  $n_c$  of the BHJ device to the unevenness of the D/A interface due to the nano-level mixing of the D and A domains<sup>15,16</sup>. Hedley *et al.*<sup>15</sup> reported that the domain (100–200 nm) of PTB7/PC<sub>71</sub>BM blend film consists of small fullerene spheres (20–60 nm) inside the domain. The resultant inhomogeneity of the interface activates only a portion of the interface to dissociate the excitons. Then, the interface inhomogeneity effectively reduces the interface area and increases  $n$  (per unit area of the interface). In addition, the inhomogeneity causes the carrier trapping at the interface region. The carrier trapping should enhance the carrier recombination probability. On the other hand, the interface of HJ device, which is prepared by vacuum evaporation process, is considered to be much smoother. Actually, the root-mean-square (RMS) of the PTB7 film is 0.32 nm (see Supplementary Fig. S7 online). Such a smooth interface is free from carrier trapping and is advantageous for the high branching ratio of the carrier escape.

## Summary

In summary, we investigated the interrelation between the instantaneous carrier density ( $n$ ) per D/A interface area and the carrier density ( $n_{\text{collected}}$ ) collected as photocurrent in PTB7/C<sub>70</sub> HJ device. By means of the time-resolved spectroscopy, we confirmed that the exciton-to-carrier conversion process takes place within  $\sim 1$  ps at the D/A interface of the PTB7/C<sub>70</sub> HJ device. We further determined the absolute magnitude of  $n$  by combination of the time-resolved and electrochemical spectroscopies. We found that the carrier recombination becomes dominant if  $n$  exceeds a critical concentration ( $n_c = 0.003$  carriers/nm<sup>2</sup>). A phenomenological rate equation with carrier recombination term ( $-\alpha n^3$ ) well reproduces the experimental relation between  $n$  and  $n_{\text{collected}}$ . We confirmed that a similar behavior is observed in the PTB7/PC<sub>71</sub>BM BHJ devices even though  $n_c$  is much lower than the value of the HJ device. Our quantitative investigation based on the HJ device demonstrates that the fast carrier escape from the interface region is indispensable for high PCE, because the carrier accumulation nonlinearly accelerates the carrier recombination process.

## Method

**Fabrication and characterization of the OSCs.** PTB7/C<sub>70</sub> HJ solar cell was fabricated with a structure of indium tin oxide (ITO)/poly-(3,4-ethylenedioxythiophene) (PEDOT): poly-(styrenesulfonate) (PSS) (40 nm)/PTB7 (18 nm)/C<sub>70</sub> (25 nm)/bathocuproine (BCP) (5 nm)/MgAg. The patterned ITO (conductivity: 10 Ω/sq) glass was pre-cleaned in an ultrasonic bath of acetone and ethanol and then treated in an ultraviolet-ozone chamber. A thin layer of PEDOT:PSS (40 nm) was spin-coated onto the ITO and dried at 110 °C for 10 min on a hot plate in air. A neat PTB7 film was spin-coated from an *o*-dichlorobenzene (*o*-DCB) solution. PTB7 was purchased from Sigma-Aldrich and used as received. The atomic force microscope (AFM) image of the PTB7 film is flat and consists of small grains less than 100 nm. Then, C<sub>70</sub> (25 nm) was deposited by vacuum evaporation. Finally, BCP and MgAg were deposited onto the active layer by conventional thermal evaporation at a chamber pressure lower than  $5 \times 10^{-4}$  Pa, which provided the devices with an active area of  $2 \times 5$  mm<sup>2</sup>.

PTB7/PC<sub>71</sub>BM BHJ solar cell was fabricated with a structure of ITO/PEDOT:PSS (40 nm)/active layer (140 nm)/LiF (1 nm)/Al. The patterned ITO glass was pre-cleaned in an ultrasonic bath of acetone and ethanol and then treated in an ultraviolet-ozone chamber. A thin layer of PEDOT:PSS (40 nm) was spin-coated onto the ITO and dried in air at 110 °C for 10 min on a hot plate. The substrate was then transferred to an N<sub>2</sub> glove box and dried again at 110 °C for 10 min on a hot plate. An *o*-DCB/1,8-diiodooctane (DIO) solution of PTB7 : PC<sub>71</sub>BM with a ratio of 2 : 3 by weight (8 : 12 mg/mL) was subsequently spin-coated onto the PEDOT:PSS surface to form an active layer. Finally, LiF (1 nm) and Al (80 nm) were deposited onto the active layer by conventional thermal evaporation at a chamber pressure lower than  $5 \times 10^{-4}$  Pa. The active area of the OSCs is  $2 \times 5$  mm<sup>2</sup>.

The  $J - V$  curves were measured using a voltage—current source/monitor under AM 1.5 solar-simulated light irradiation of  $100 \text{ mW/cm}^2$  (Bunkou-keiki, OTENTO-SUN III). The IPCE spectra was measured using a SM-250 system (Bunkou-keiki). The magnitudes of  $\Phi_{IQ}$  at 400 nm were evaluated from the IPCE spectra with considering the absorption indexes: 0.61 and 0.84 for the HJ and BHJ devices, respectively.

**Pulse energy dependence of  $\Phi_{IQ}$  of the OSCs.** The pulse energy dependences of  $\Phi_{IQ}$  of the OSCs were measured in a  $\text{N}_2$ -filled box. For this experiment, the active area of the OSCs is  $2 \times 3 \text{ mm}^2$ . The excitation light pulse at 400 nm was generated as the second harmonics of a regenerative amplified Ti: sapphire laser in a  $\beta\text{-BaB}_2\text{O}_4$  (BBO) crystal. The pulse width and repetition rate were 100 fs and 500 Hz, respectively. The maximum excitation intensity was  $27 \mu\text{J/cm}^2$ . The photocurrents ( $I$ ) from the OSCs were measured against the excitation pulse energy ( $I_{\text{photon}}$ ) per unit area of the device. The magnitudes of  $\Phi_{IQ}$  were evaluated by  $I$  and  $I_{\text{photon}}$ , with considering the absorption indexes: 0.61 and 0.84 for the HJ and BHJ devices, respectively.

**Femtosecond time-resolved spectroscopy.** The time-resolved spectroscopy was performed in a pump-probe configuration. In order to reduce the irradiation damage, the blend films were placed in  $\text{N}_2$  atmosphere. The pump pulse at 400 nm was generated as the second harmonics of a regenerative amplified Ti: sapphire laser in a  $\beta\text{-BaB}_2\text{O}_4$  (BBO) crystal. The pulse width, repetition rate, and pulse energy were 100 fs, 1000 Hz, and  $27 \mu\text{J/cm}^2$  respectively. The frequency of the pump pulse was decreased by half (500 Hz) to provide “pump-on” and “pump-off” conditions. A white probe pulse, generated by self-phase modulation in a sapphire plate was focused on the sample with the pump pulse. The spot sizes of the pump and probe pulses were 4.0 and 2.1 mm in diameter, respectively. The differential absorption ( $\Delta\text{OD}$ ) spectrum is expressed as  $-\log(I_{\text{on}}/I_{\text{off}})$ , where  $I_{\text{on}}$  and  $I_{\text{off}}$  are the transmission spectra under the pump-on and pump-off conditions, respectively.

Films prepared on quartz substrates were used in the time-resolved spectroscopies. PTB7/ $C_{70}$  bilayer film was prepared as follows. First, PTB7 neat film (18 nm) was spin-coated on quartz substrate from an *o*-DCB solution. The spin-coated film was dried in an inert  $\text{N}_2$  atmosphere. Then,  $C_{70}$  (25 nm) was deposited by vacuum evaporation. PTB7/ $PC_{71}\text{BM}$  blend film was spin-coated on quartz substrate from a mixed solvent of *o*-DCB /DIO (97.5 : 2.5 vol %) of PTB7 :  $PC_{71}\text{BM}$  with a ratio of 2 : 3 by weight (8 : 12 mg/mL). PTB7 neat film was spin-coated on quartz substrate from *o*-DCB solution. The spin-coated films were dried in an inert  $\text{N}_2$  atmosphere. The thicknesses of the PTB7 and PTB7/ $PC_{71}\text{BM}$  blend films were 100 and 140 nm, respectively.

**Pulse energy dependence of  $\Phi_{CF}$ .** The magnitude of  $\Phi_{CF}$  ( $=\alpha_{\text{photon}}/\alpha_{D^+}$ ) can be calculated from the two quantities.  $\alpha_{D^+}$  ( $\alpha_{\text{photon}}$ ) is the spectral intensity due to  $D^+$  per unit density of  $D^+$  (absorbed photons).  $\alpha_{D^+}$  is reported to be  $0.013 \text{ nm}^2/\text{carriers}$  for PTB7<sup>13</sup>. In the PTB7-based OSCs, the carrier formation time is less than 1 ps. Therefore, we evaluated the  $\alpha_{D^+}$  values from the  $\Delta\text{OD}$  spectra at 10 ps of the PTB7/ $C_{70}$  bilayer and PTB7/ $PC_{71}\text{BM}$  blend films with considering the absorption indexes: 0.37 and 0.60 for the bilayer and blend films, respectively.

## References

- Gregg, B. A. & Hanna, M. C. Comparing organic photovoltaic cells; Theory, experiment, and simulation. *J. Appl. Phys.* **93**, 3605–3614 (2003).
- Hiramoto, M., Fujiwara, H. & Yokoyama, M. Three-layered organic solar cell with a photoactive interlayer of codeposited pigments. *Appl. Phys. Lett.* **58**, 1062–1064 (1991).
- Sariciftci, N. S., Smilowitz, L., Heeger, A. J. & Wudl, F. Photoinduced electron transfer from a conducting polymer to buckminsterfullerene. *Science* **285**, 1474–1476 (1992).
- He, Z. *et al.* Enhanced power-conversion efficiency in polymer solar cells using an inverted device structure. *Nature Photon* **6**, 591–595 (2012).
- Nguyen, T. L. *et al.* Semi-crystalline photovoltaic polymers with efficiency exceeding 9% in a  $\sim 300 \text{ nm}$  thick conventional single-cell device. *Energy Environ. Sci.* **7**, 3040–3051 (2014).
- Guo, X. *et al.* Enhanced photovoltaic performance by modulating surface composition in bulk heterojunction polymer solar cells based on PBDTTT-C-T/ $PC_{71}\text{BM}$ . *Adv. Mater.* **26**, 4043–4049 (2014).
- He, Z. *et al.* Simultaneous enhancement of open-circuit voltage, short-circuit current density, and fill factor in polymer solar cells. *Adv. Mater.* **23**, 4636–4643 (2011).
- Szarko, J. M., Guo, J.-C., Rolczynski, B. S. & Chen, L. X. Current trends in the optimization of low band gap polymers in bulk heterojunction photovoltaic devices. *J. Mater. Chem.* **21**, 7849–7857 (2011).
- Yonezawa, K., Kamioka, H., Yasuda, T., Han, L. & Moritomo, Y. Fast carrier formation from acceptor exciton in low-gap organic photovoltaic. *Appl. Phys. Express* **5**, 042302 (2012).
- Yonezawa, K., Kamioka, H., Yasuda, T., Han, L. & Moritomo, Y. Exciton-to-carrier conversion processes in a low-band-gap organic photovoltaic. *Jpn. J. Appl. Phys.* **52**, 062405 (2013).
- Guo, J. *et al.* Structure, dynamics, and power conversion efficiency correlations in a new low bandgap polymer: PCBM solar cell. *J. Phys. Chem. B* **114**, 742–748 (2010).
- Rolczynski, B. S. *et al.* Ultrafast intramolecular exciton splitting dynamics in isolated low-band-gap polymers and their implications in photovoltaic materials design. *J. Am. Chem. Soc.* **134**, 4142–4152 (2012).
- Moritomo, Y., Yonezawa, K. & Yasuda, T. Effect of temperature on carrier formation efficiency in organic photovoltaic cells. *Appl. Phys. Lett.* **105**, 073902 (2014).
- Marsh, R. A., Hodgkiss, J. M., Albert-Seifried, S. & Friend, R. H. Effect of Annealing on P3HT:PCBM Charge Transfer and Nanoscale Morphology Probed by Ultrafast Spectroscopy. *Nano Lett.* **10**, 923–930 (2010).

15. Hedley, G. J. *et al.* Determining the optimum morphology in high-performance polymer-fullerene organic photovoltaic cells. *Nature Commun.* **4**, 2867 (2013).
16. Kesava, S. V. *et al.* Domain composition and fullerene aggregation govern charge photogeneration in polymer/fullerene solar cells. *Adv. Energy Mater.* **4**, 1400116 (2014).

### Acknowledgements

This work was partially supported by a Grant-in-Aid (No. 23684022) for Scientific Research from the Ministry of Education, Culture, Sports, Science and Technology, Japan.

### Author Contributions

Y.M. planned overall the investigation and wrote the manuscript. T.Y. fabricated and characterized the organic solar cells. He further measured the photon flux dependence of  $\Phi_{IQ}$ . K.Y. performed femtosecond time-resolved spectroscopies and analyzed the exciton-to-carrier conversion process. He further determined the photon flux dependence of  $\Phi_{CF}$ .

### Additional Information

**Supplementary information** accompanies this paper at <http://www.nature.com/srep>

**Competing financial interests:** The authors declare no competing financial interests.

**How to cite this article:** Moritomo, Y. *et al.* Carrier density effect on recombination in PTB7-based solar cell. *Sci. Rep.* **5**, 13648; doi: 10.1038/srep13648 (2015).



This work is licensed under a Creative Commons Attribution 4.0 International License. The images or other third party material in this article are included in the article's Creative Commons license, unless indicated otherwise in the credit line; if the material is not included under the Creative Commons license, users will need to obtain permission from the license holder to reproduce the material. To view a copy of this license, visit <http://creativecommons.org/licenses/by/4.0/>